Figure 3.1 **CO_2 emissions, SO_2 emissions, and atmospheric CO_2 concentration through 2100 for the six "Marker/Illustrative" SRES scenarios and the IS92a scenario (a "business as usual" scenario, IPCC (1992)). (Source: IPCC 2001)**

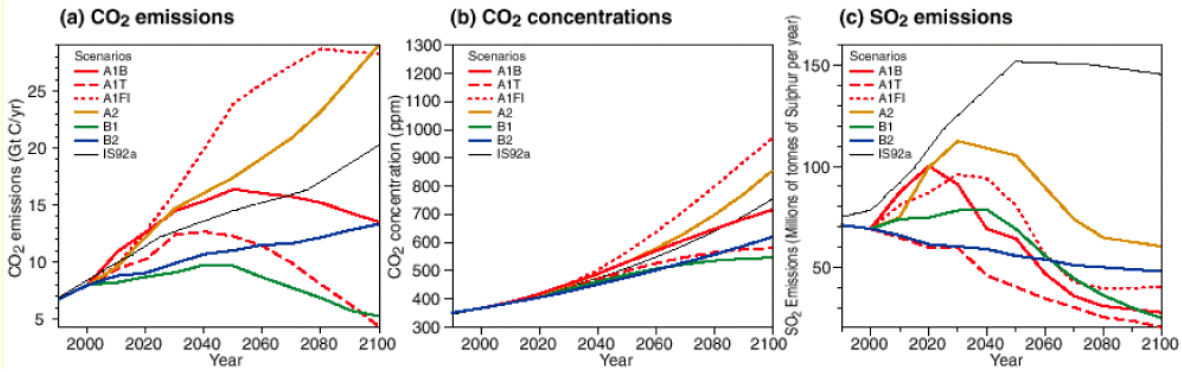

Figure 3.2 **United States Climate Divisions of the central Gulf Coast study area. Empirical trends and variability were analyzed for temperature and precipitation at the Climate Division Dataset (CDD) level for the climate divisions along the Gulf Coast from Galveston to Mobile, including Texas Climate Division 8, Louisiana Divisions 6-9, Mississippi Division 10, and Alabama Division 8. These climatic divisions cover the entire central Gulf Coast study area.**

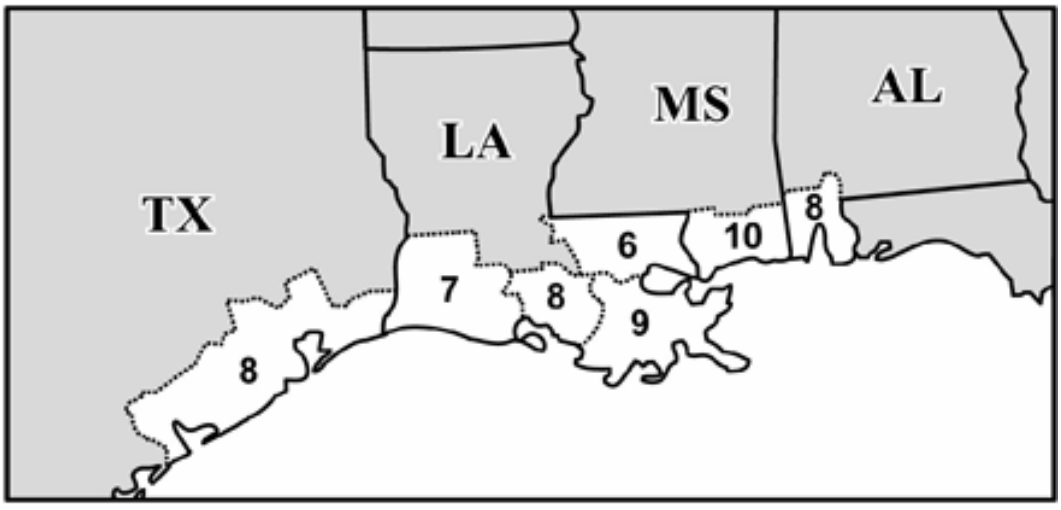

Figure 3.3 Grid area for the GCM temperature and precipitation results presented in Section 3.15 of this report, which is a subset of the global grid of a typical GCM output.

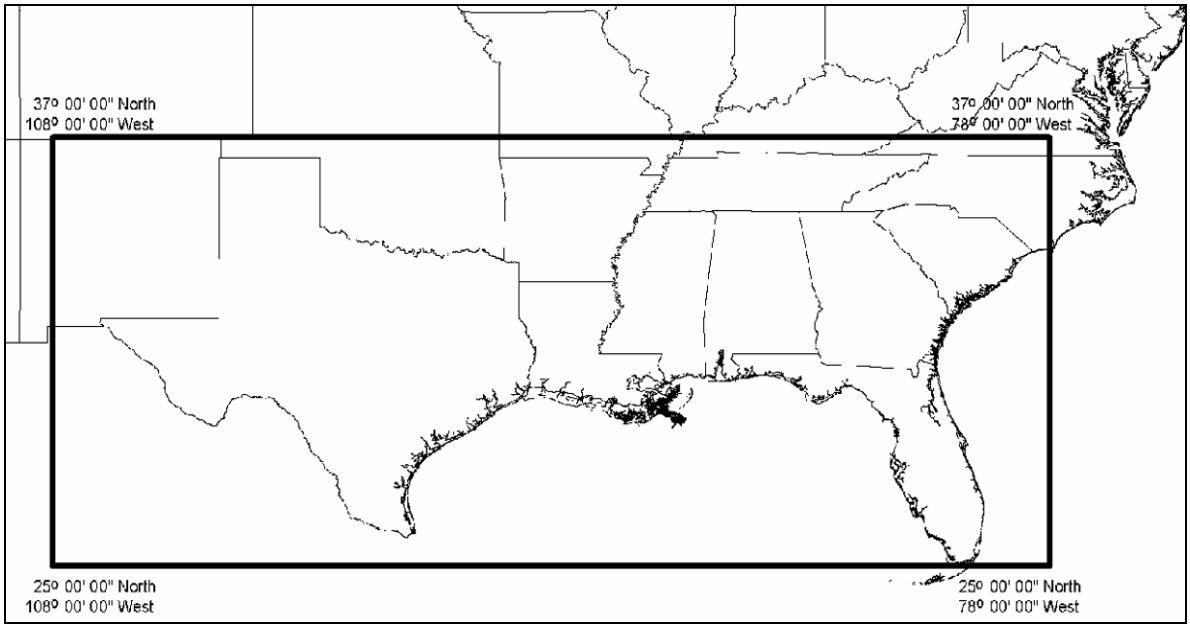

Figure 3.4 Scatterplot of seasonal temperature and precipitation predictions by an ensemble of GCMs for the Gulf Coast region in 2050 using the SRES A1B emissions scenario.

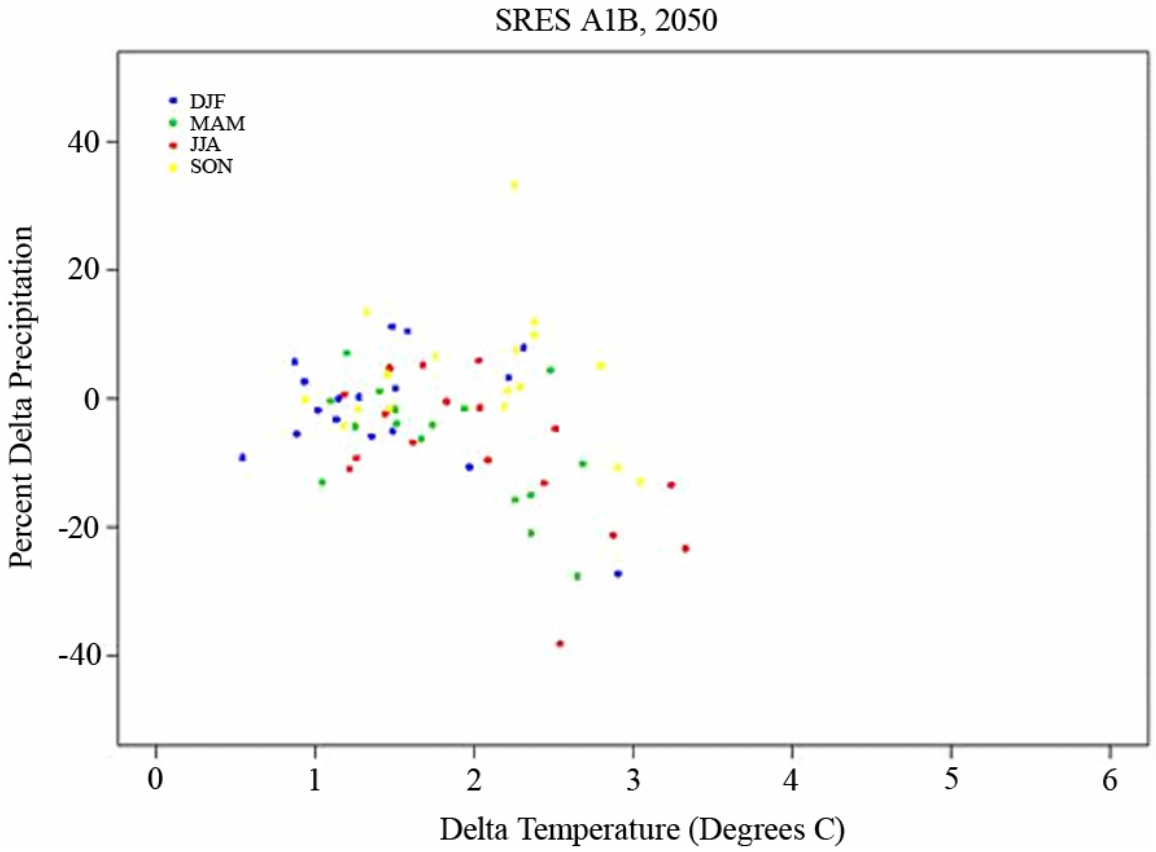

Figure 3.5 Temperature variability from 1905-2003 for the 7 Climate Divisions making up the Gulf Coast study area.

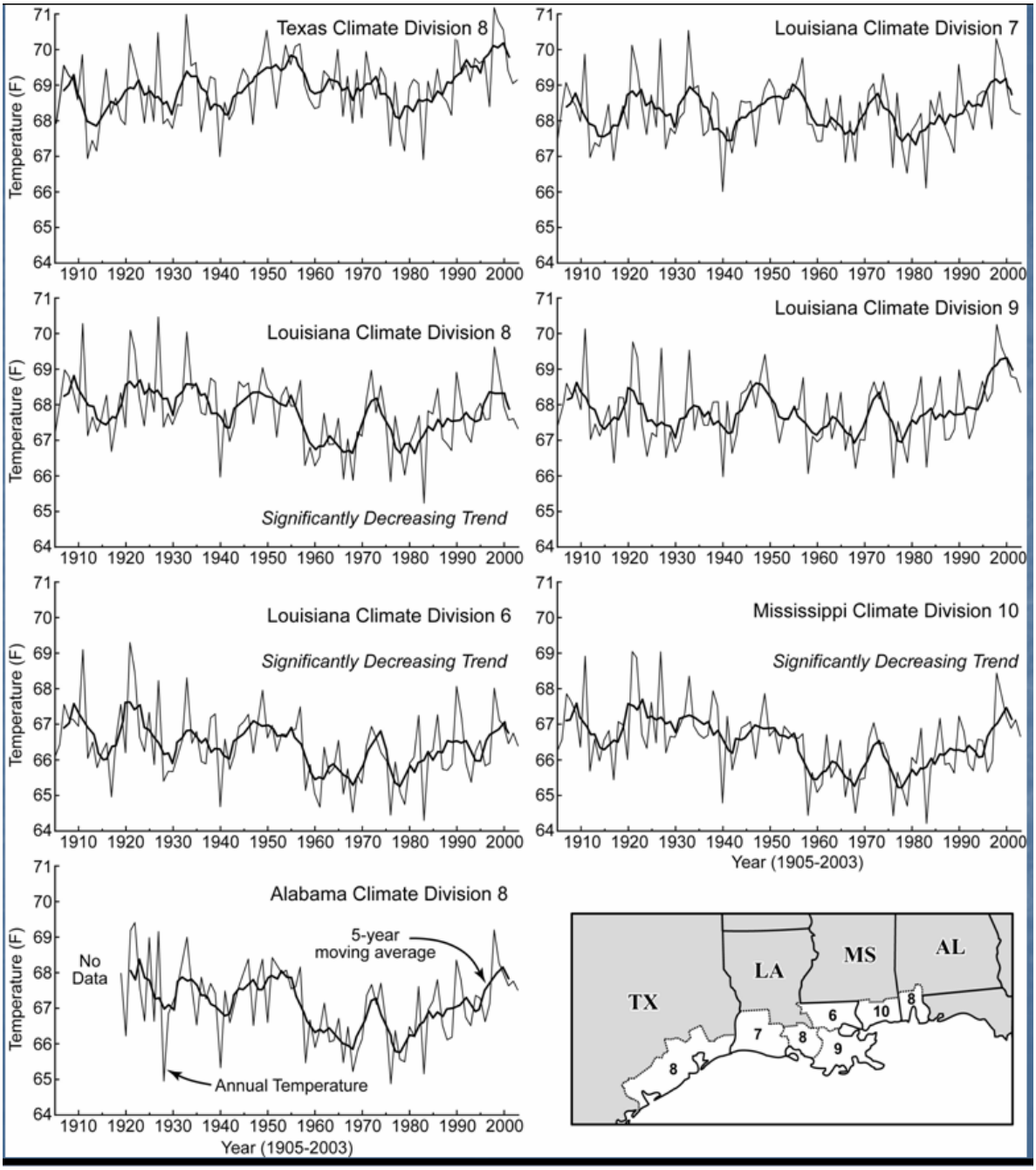

Figure 3.6 Precipitation variability from 1905 to 2003 for the seven Climate Divisions making up the Gulf Coast study area.

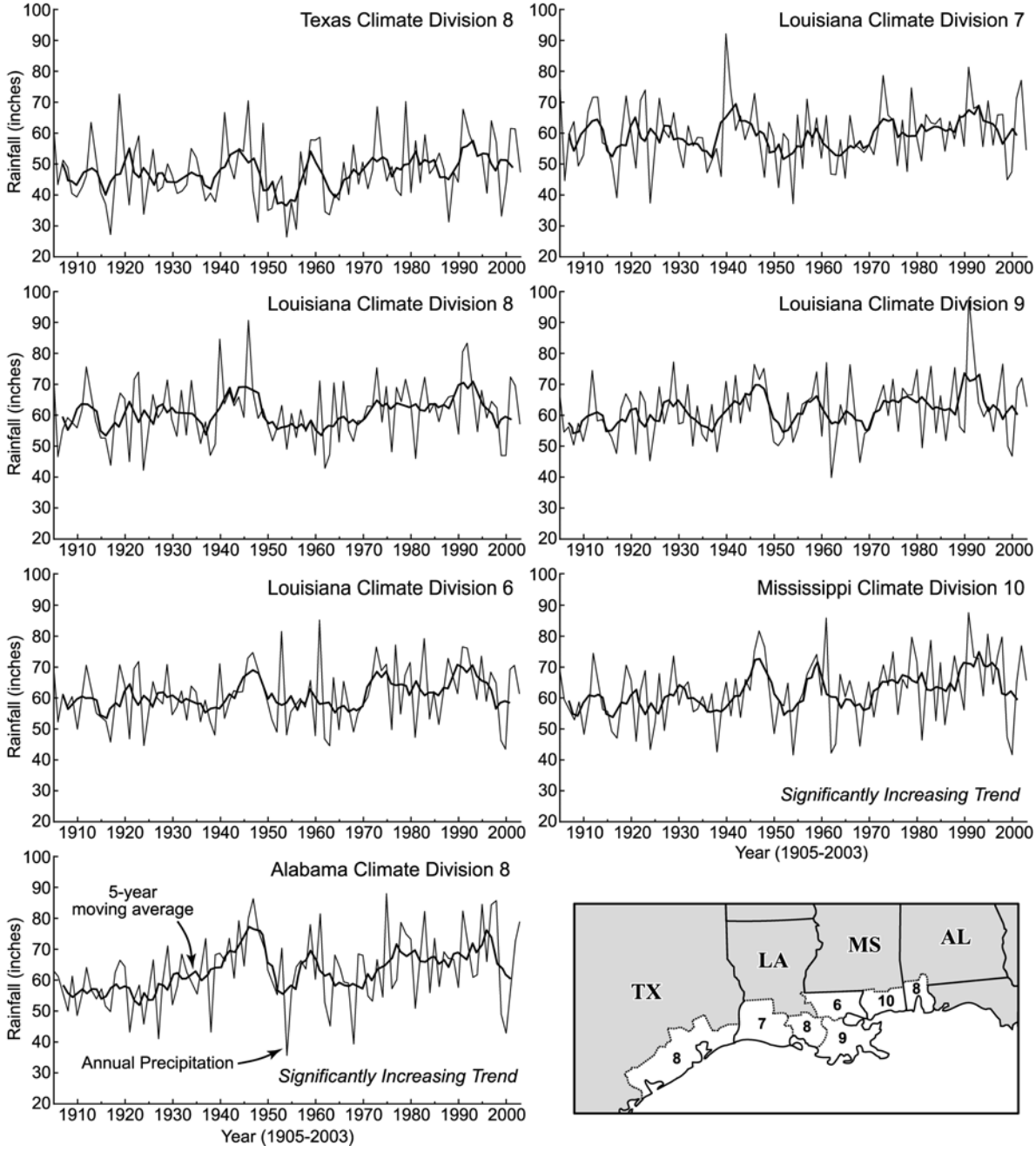

Figure 3.7 Variability and trends in model-derived surplus (runoff) and deficit from 1919 to 2003 for the Gulf Coast study area.

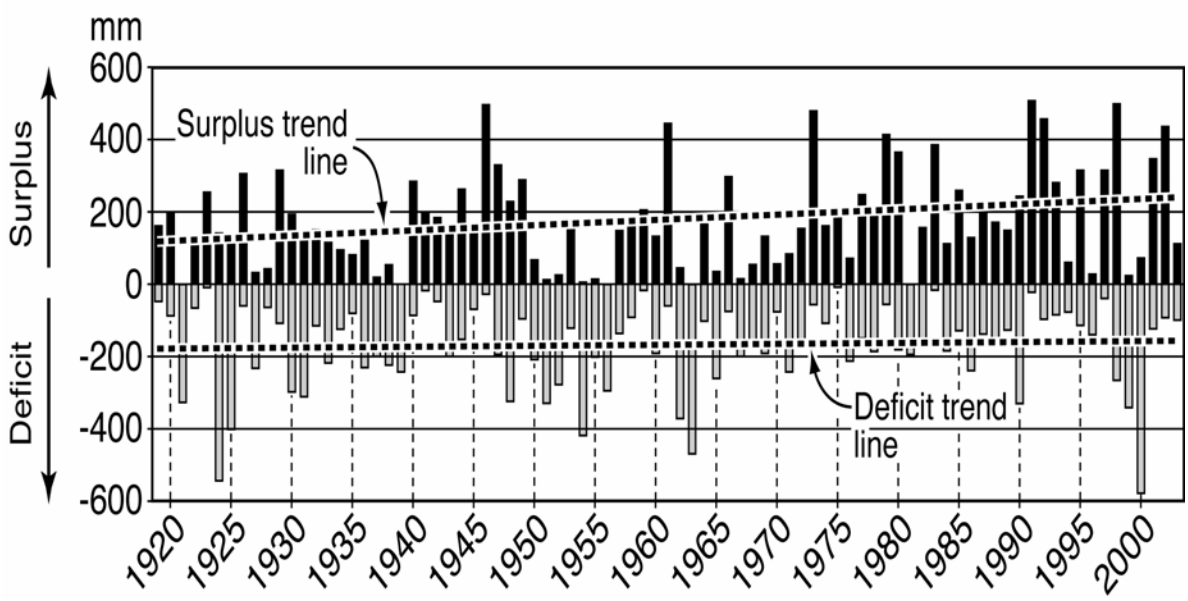

Figure 3.8 Probability density functions for seasonal temperature change (in °C) in the Gulf Coast study area for 2050 using the A1B emissions scenario.

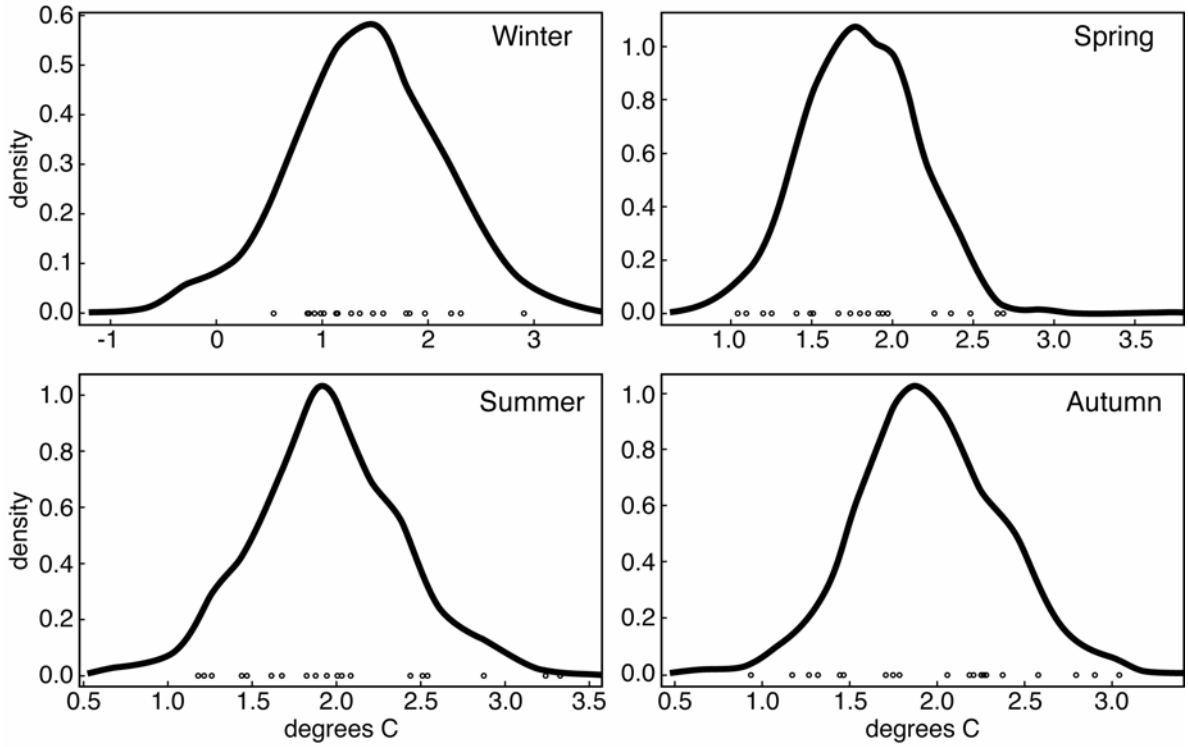

Figure 3.9 Probability density functions for seasonal precipitation change (in percent) in the U.S. Gulf Coast study area for 2050 using the A1B emissions scenario.

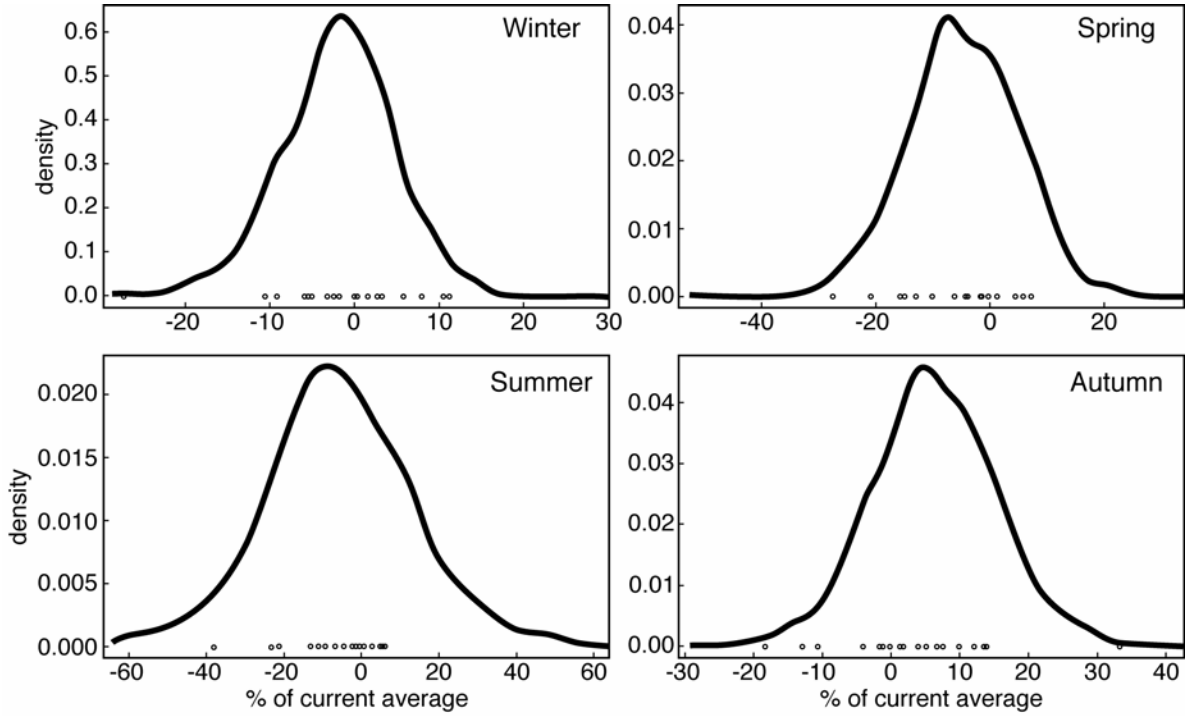

Figure 3.10 Quantile estimates of monthly precipitation for the 2- to 100-year return period using the 1971 to 2000 baseline period relative to GCM output for the A1B emissions scenario at the 5%, 50%, and 95% quartiles.

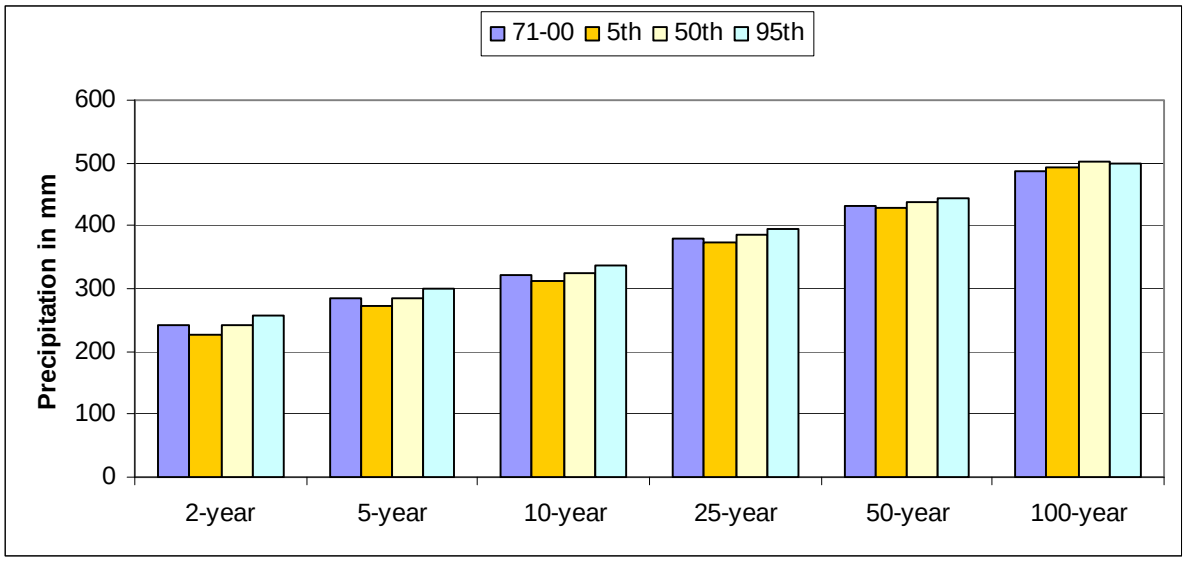

Figure 3.11 Quantile estimates of monthly average runoff for the 2- to 100-year return period using the 1971 to 2000 baseline period relative to GCM output for the A1B emissions scenario at the 5%, 50%, and 95% quartiles.

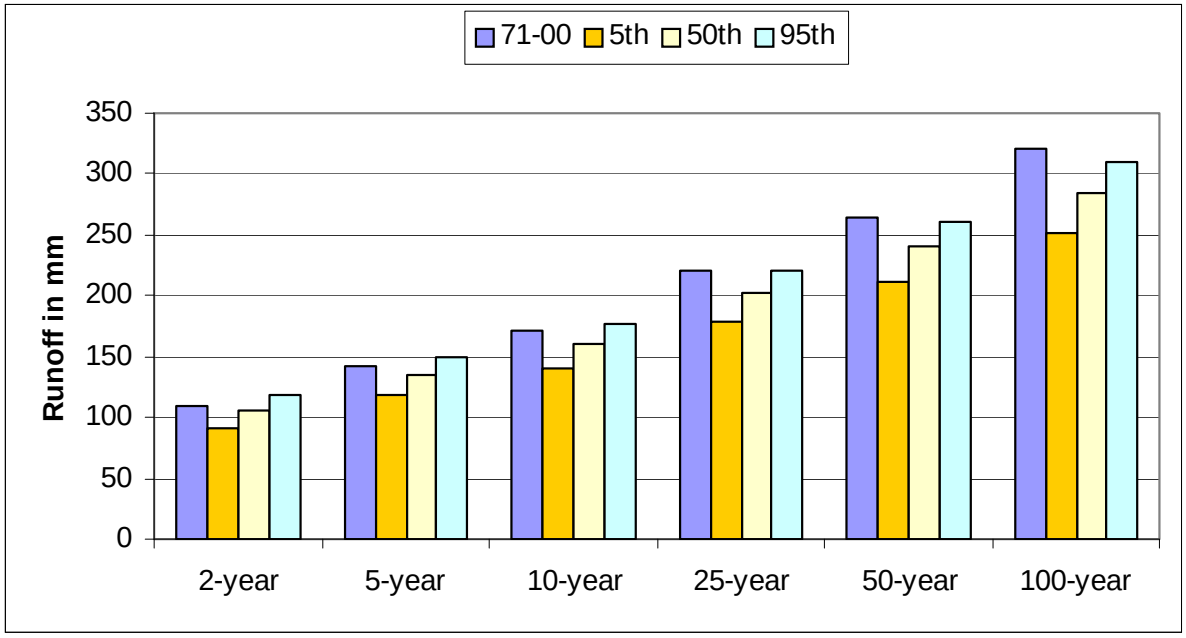

Figure 3.12 Quantile estimates of monthly average deficit for the 2- to 100-year return period using the 1971 to 2000 baseline period relative to GCM output for the A1B emissions scenario at the 5%, 50%, and 95% quartiles.

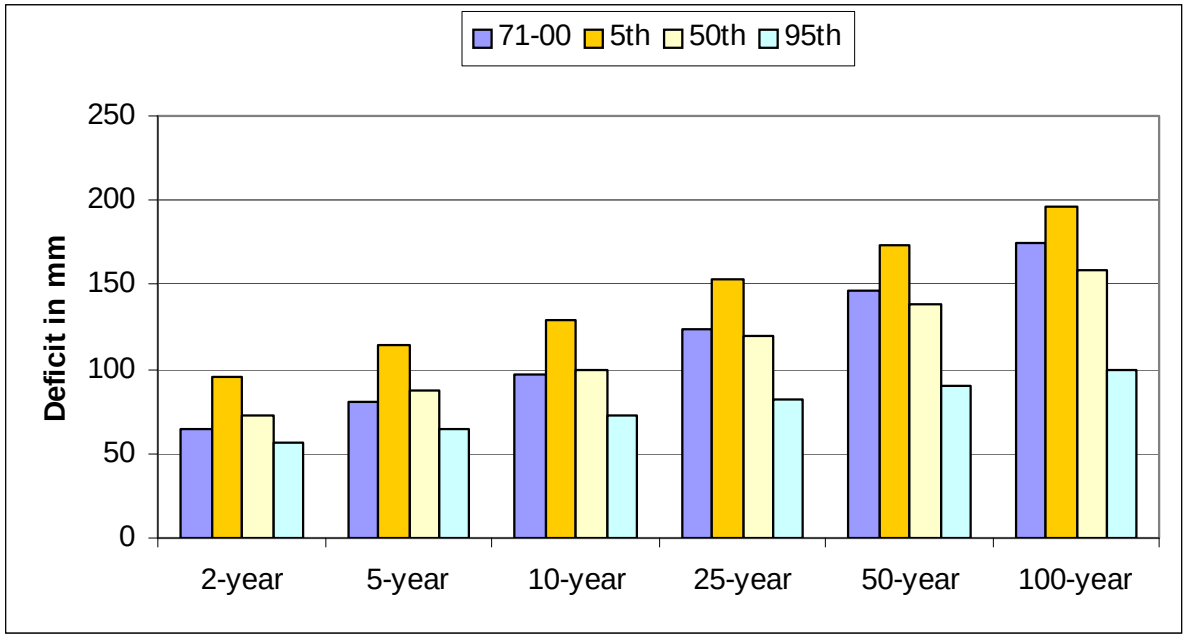

Figure 3.13 The change in the warmest 10% of July maximum and minimum temperatures at each station across the entire United States, for 1950-2004. Note the number of days above the 90th percentile in minimum temperature is rising faster than maximum temperature.

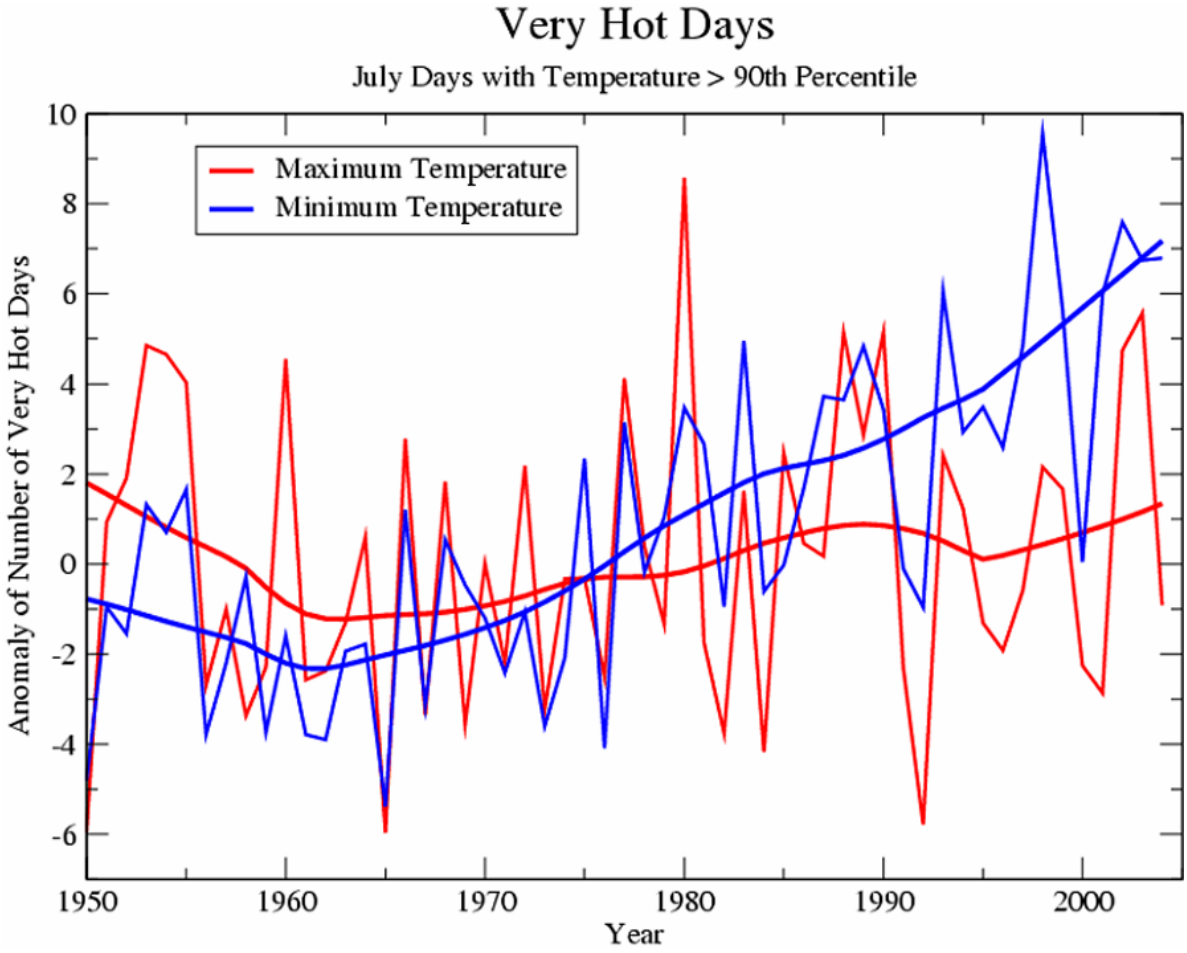

Figure 3.14 Historical time series from stations within 500 km of the Dallas, Texas showing anomalies of the number of days above 37.7°C (100°F), for 1950-2004.

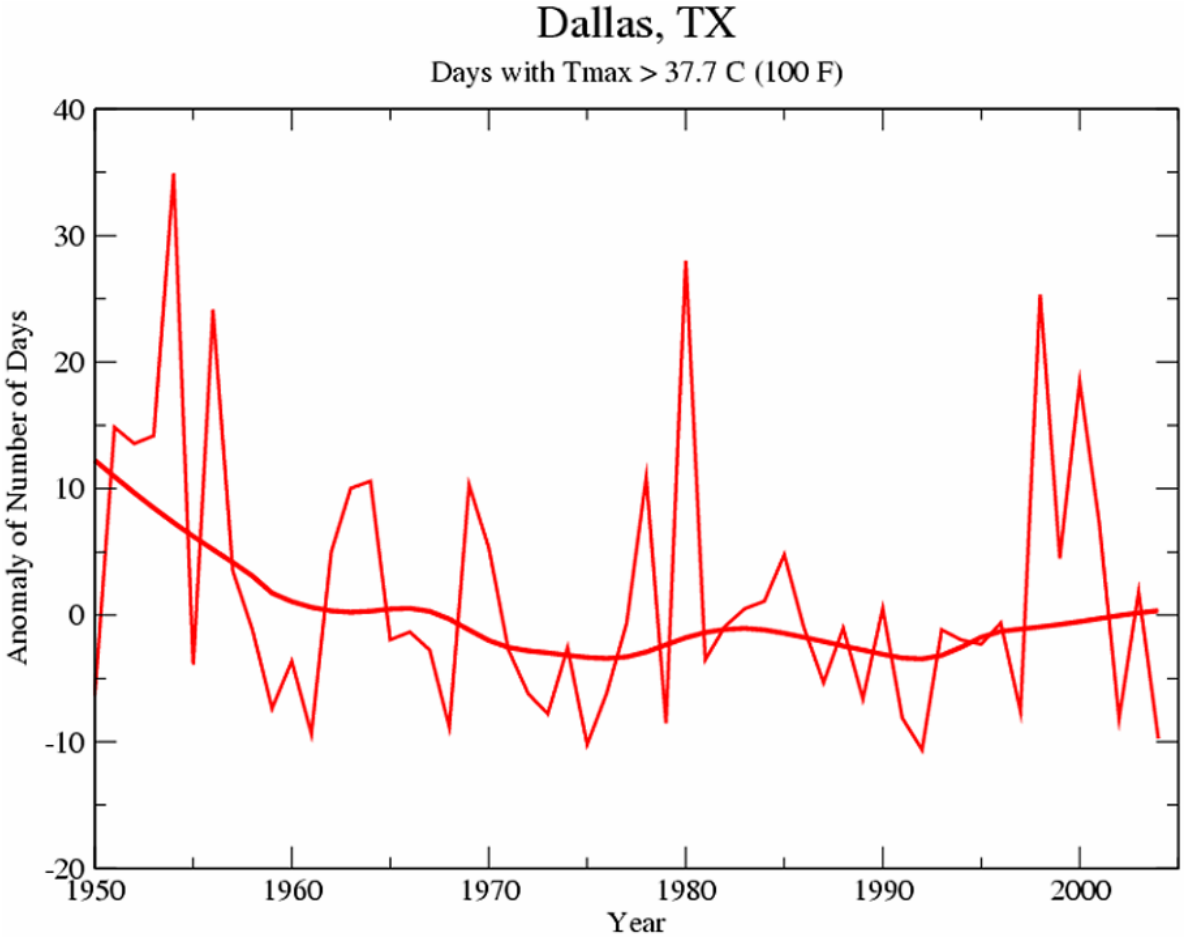

Figure 3.15 The current and future probabilities of having one to twenty days during the summer at or above 37.8°C (100°F) in or near Houston, Texas under the A2 emissions scenario.

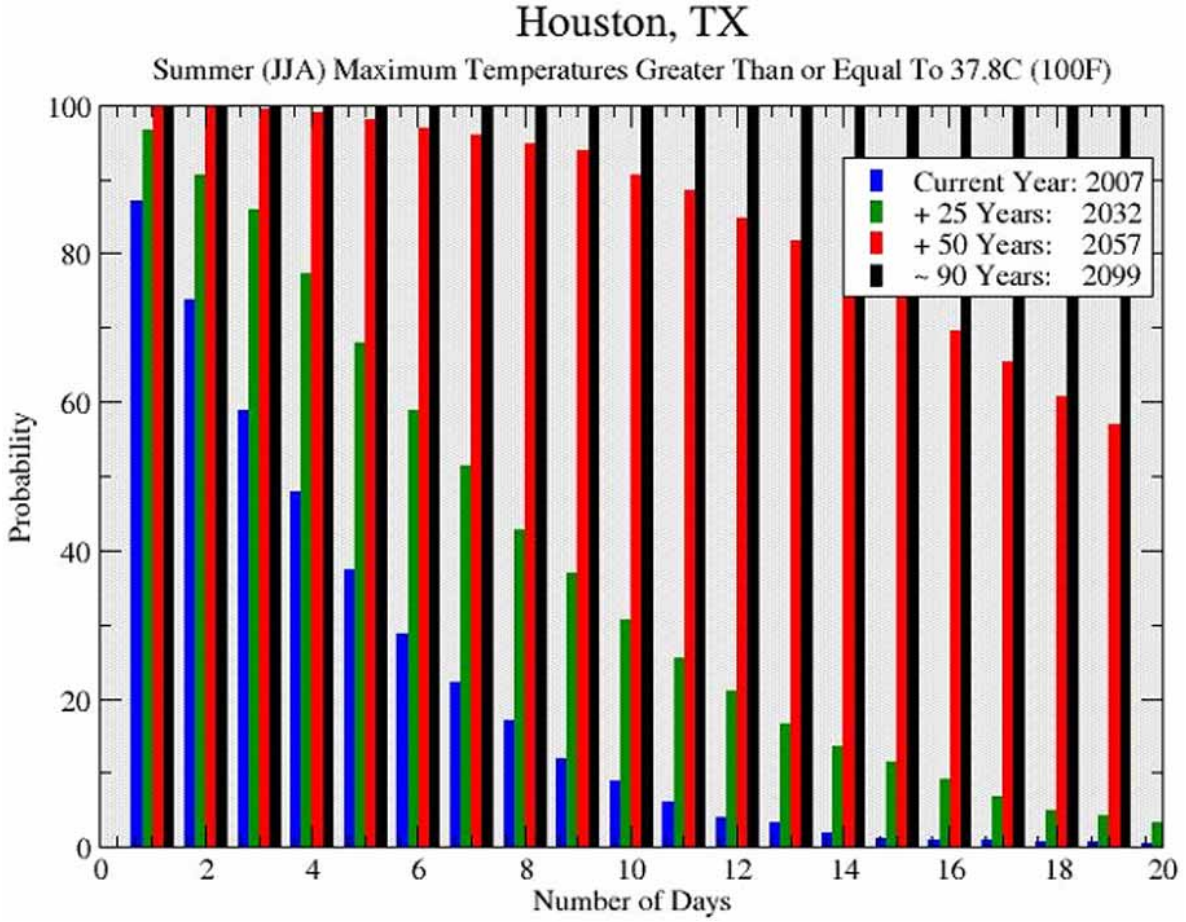

Figure 3.16 Mean model predicted change (Celsius) of the 20-year return value of the annual maximum daily averaged surface air temperature under the A1B emissions scenario in the Gulf States region. This analysis compares the 1990-1999 period to the 2090-2099 period.

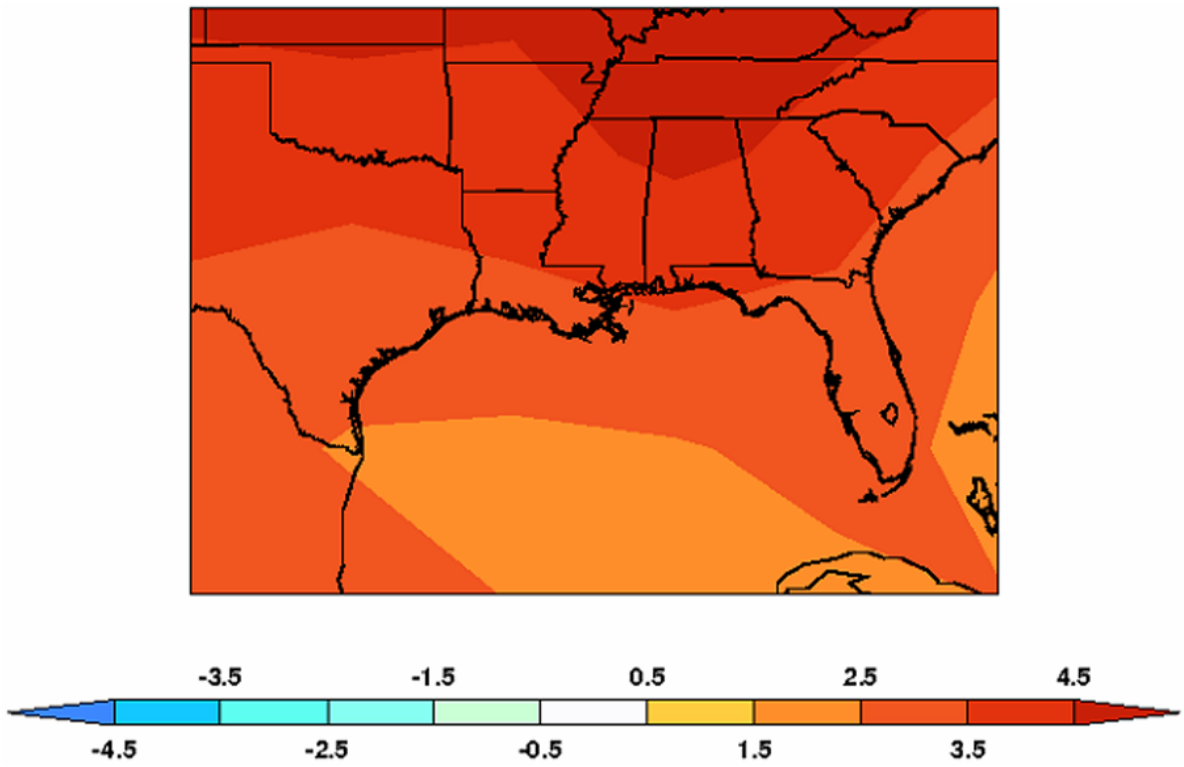

Figure 3.17 Number of times on average over a 20-year period that the 1990-1999 annual maximum daily averaged surface air temperature 20-year return value levels would be reached under the SRES A1B 2090-2099 forcing conditions over 20 years. Under 1990-1999 forcing conditions, this value is defined to be one.

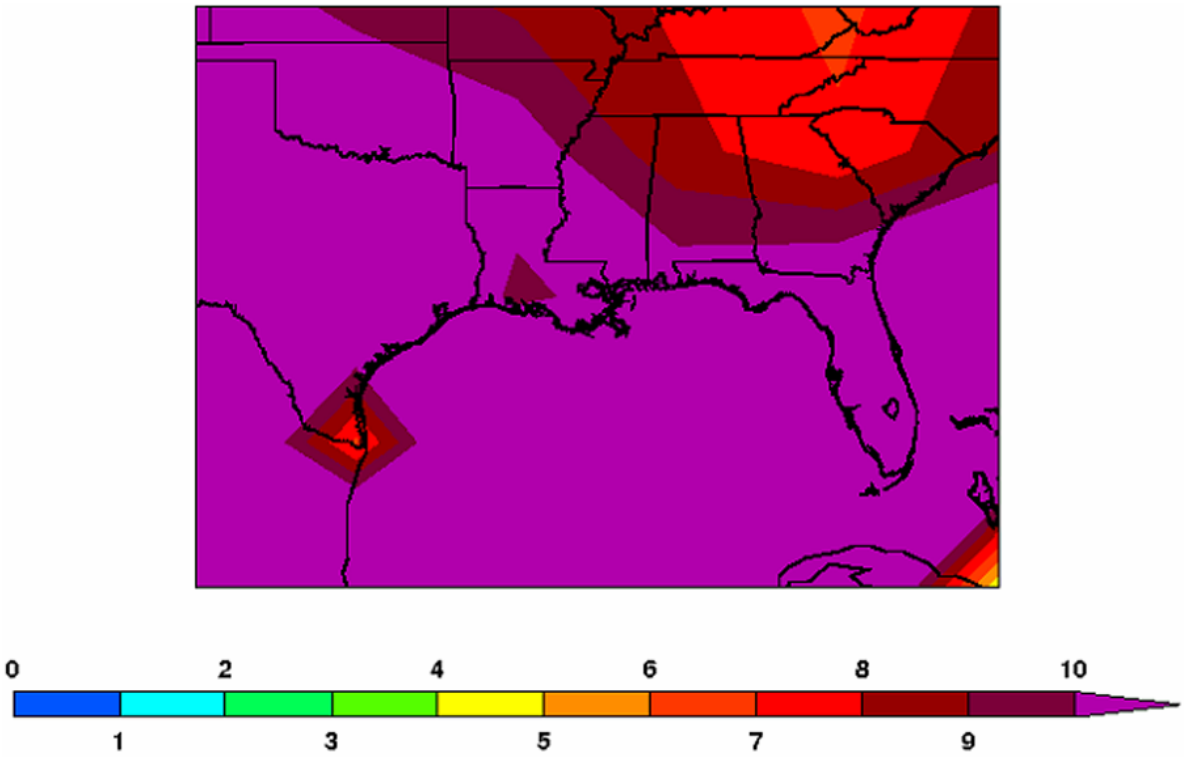

Figure 3.18 Mean model predicted fractional change of the 20-year return value of the annual maximum daily averaged precipitation under the SRES A1B in the Gulf States region. This analysis compares the 1990-1999 period to the 2090-2099 period.

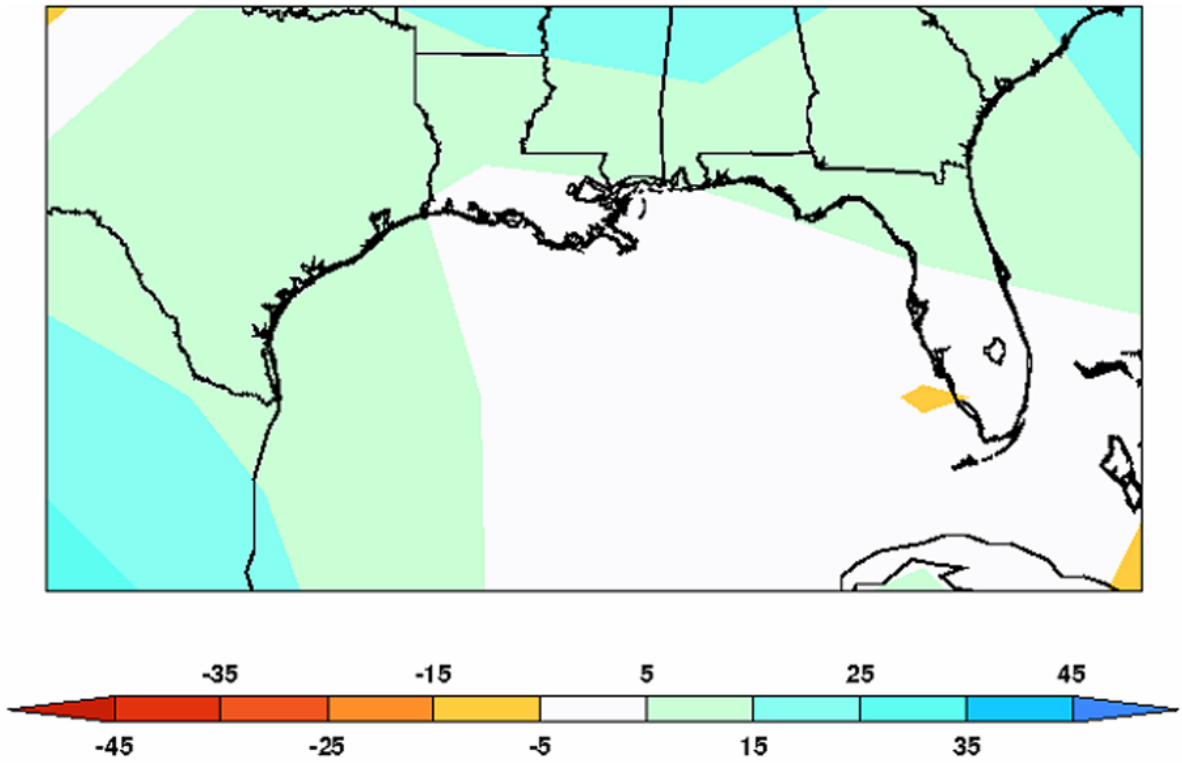

Figure 3.19 Geographic distribution of hurricane landfalls along the Atlantic and Gulf Coast region of the U.S., from 1950 to 2006. (Source: NOAA, National Climate Data Center, Asheville, N.C.)

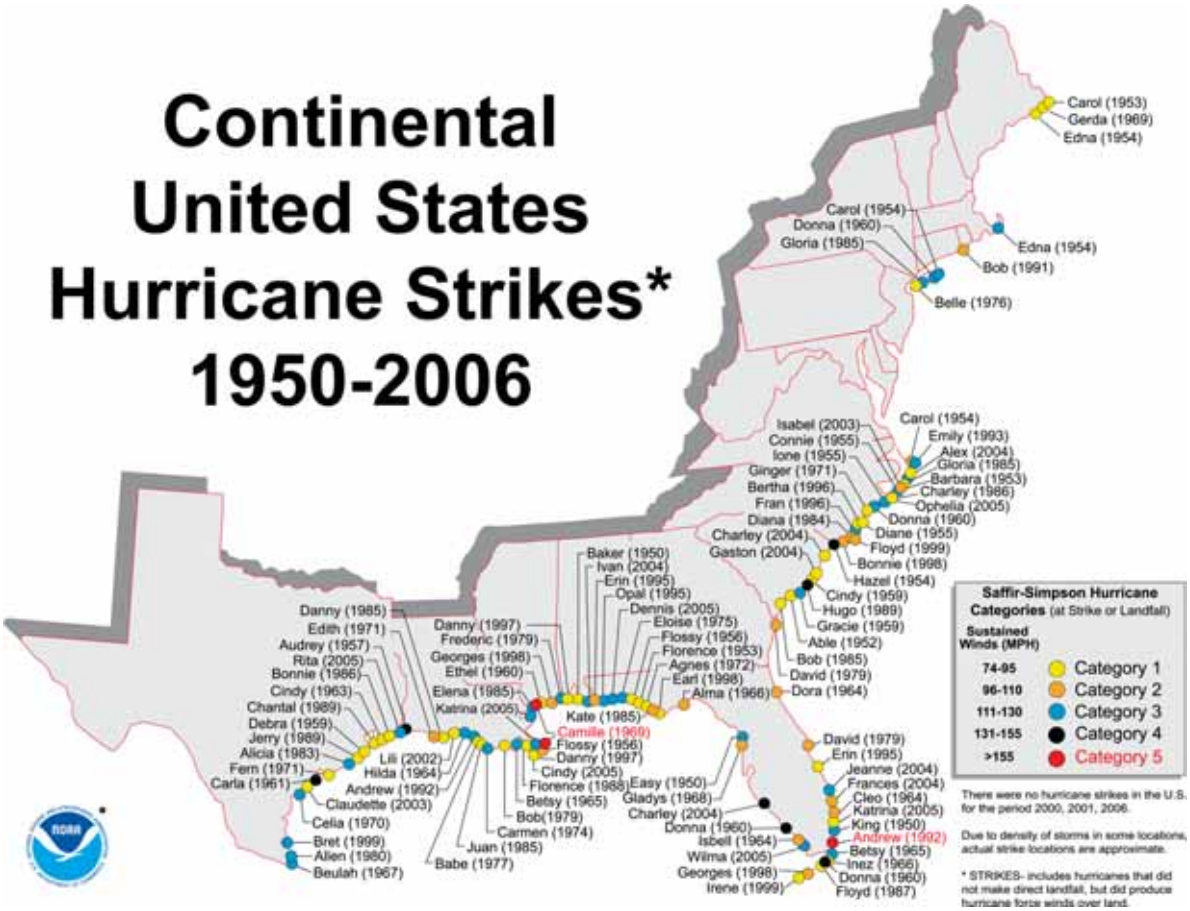

Figure 3.20 Frequency histogram of landfalling storms of tropical storm strength or greater in Grand Isle, Louisiana summarized on a 5 year basis, for the period 1851-2005. (Source: NOAA National Hurricane Research Division)

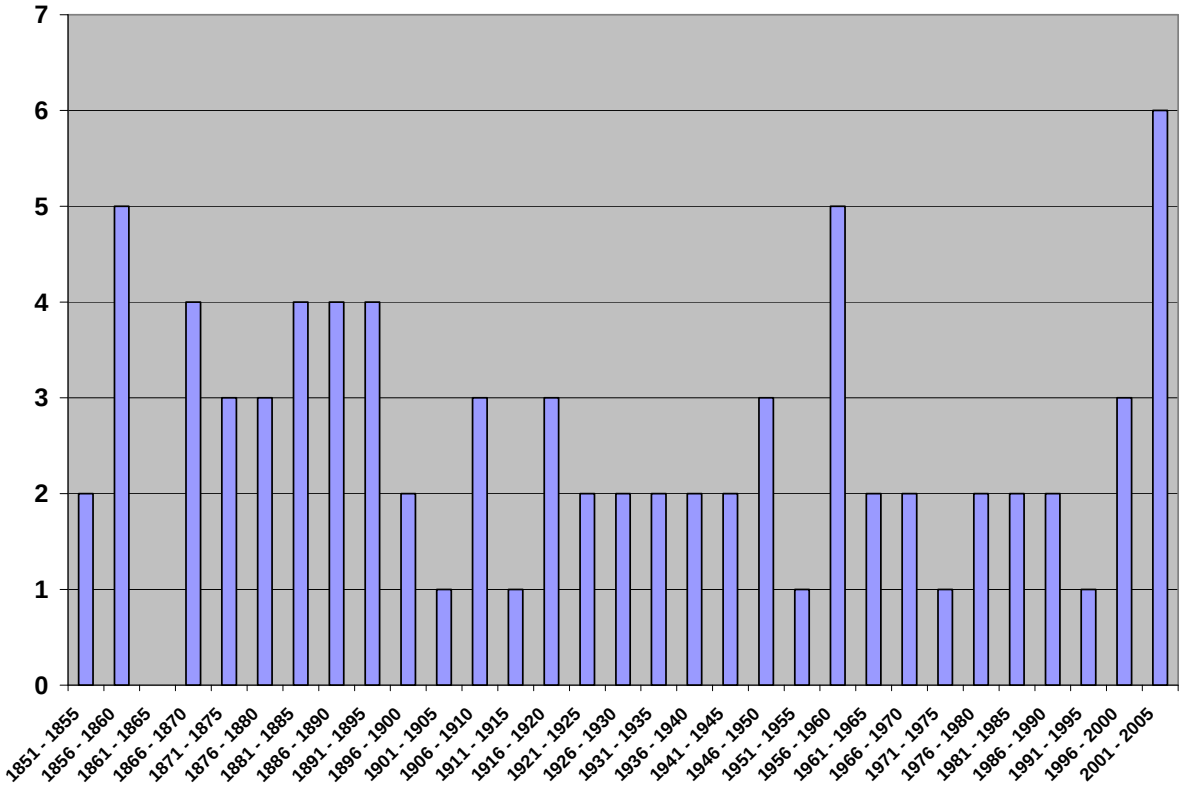

Figure 3.21 Hemispherical and global mean sea-surface temperatures for the period of record 1855 to 2000. (Source: NOAA, National Climate Data Center, Asheville, N.C.)

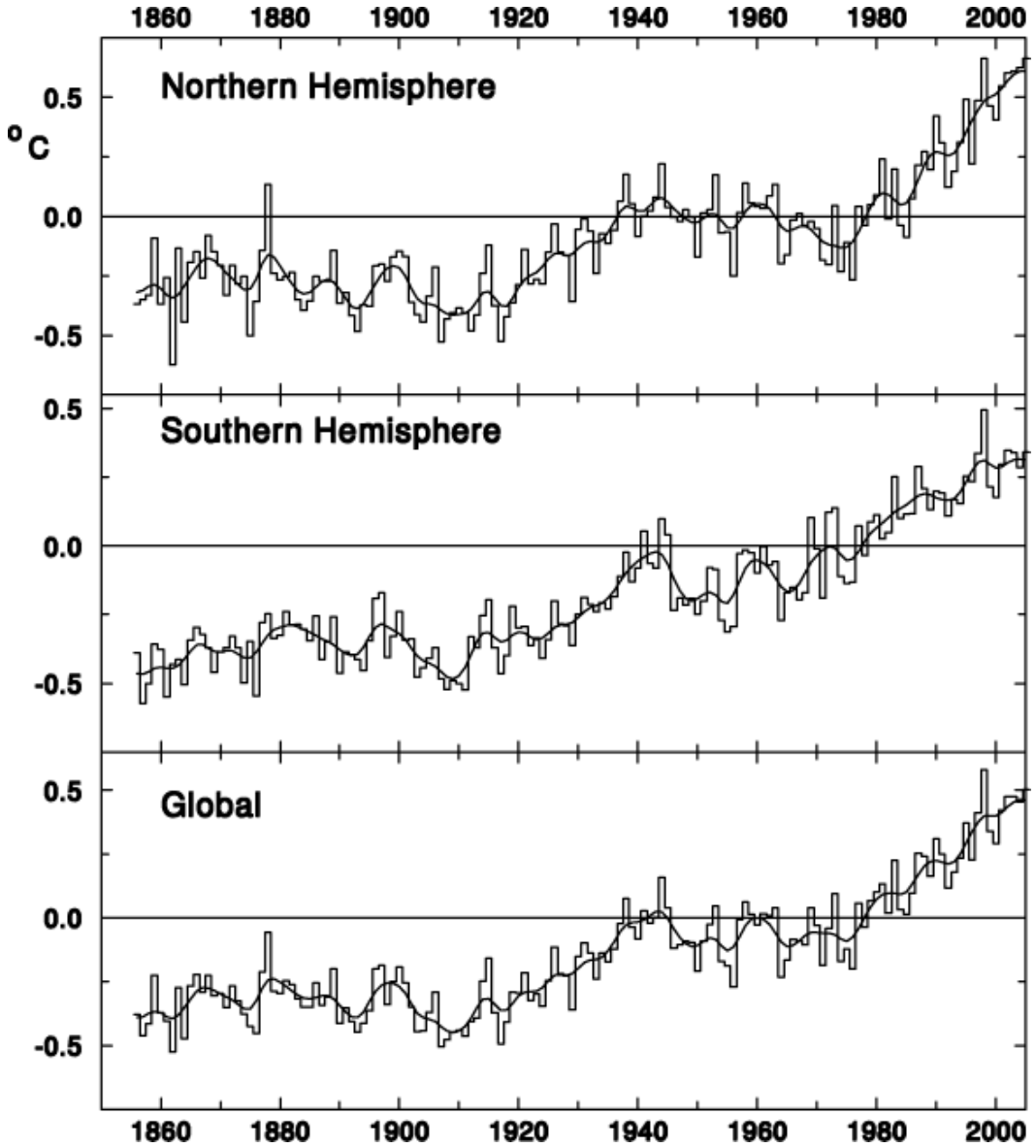

Figure 3.22 Sea surface temperature trend in the main hurricane development region of the North Atlantic during the past century. Red line shows the corresponding 5-yr running mean. Anomalies are departures from the 1971–2000 period monthly means. (Source: Bell *et al.* 2007)

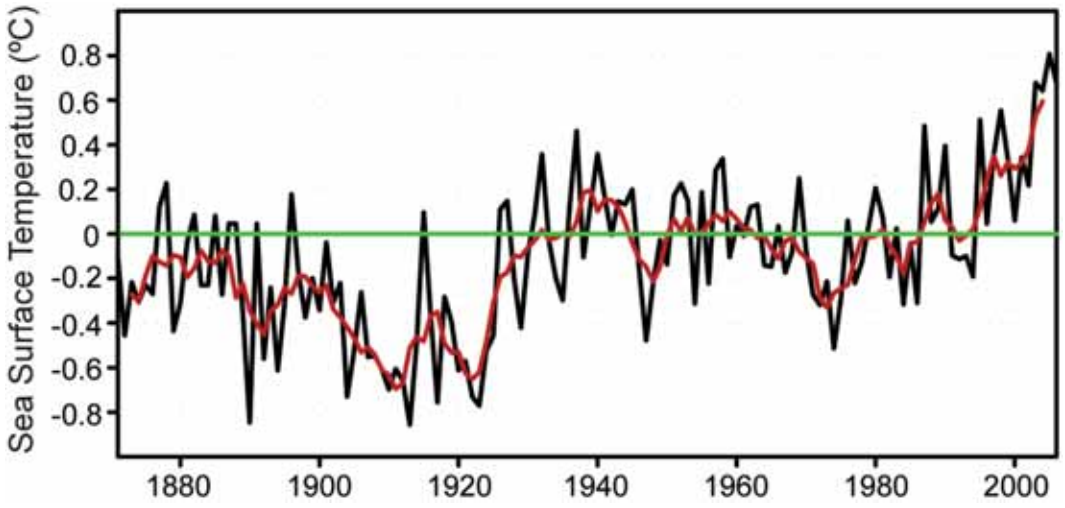

Figure 3.23 Sea surface temperature trend in the Gulf of Mexico region produced using the ERSST v.2 database. The plot includes the SST anomalies averaged annually, as well as the anomalies determined from the averages for August only and the July-September peak of the hurricane season. (Source: Smith and Reynolds, 2004)

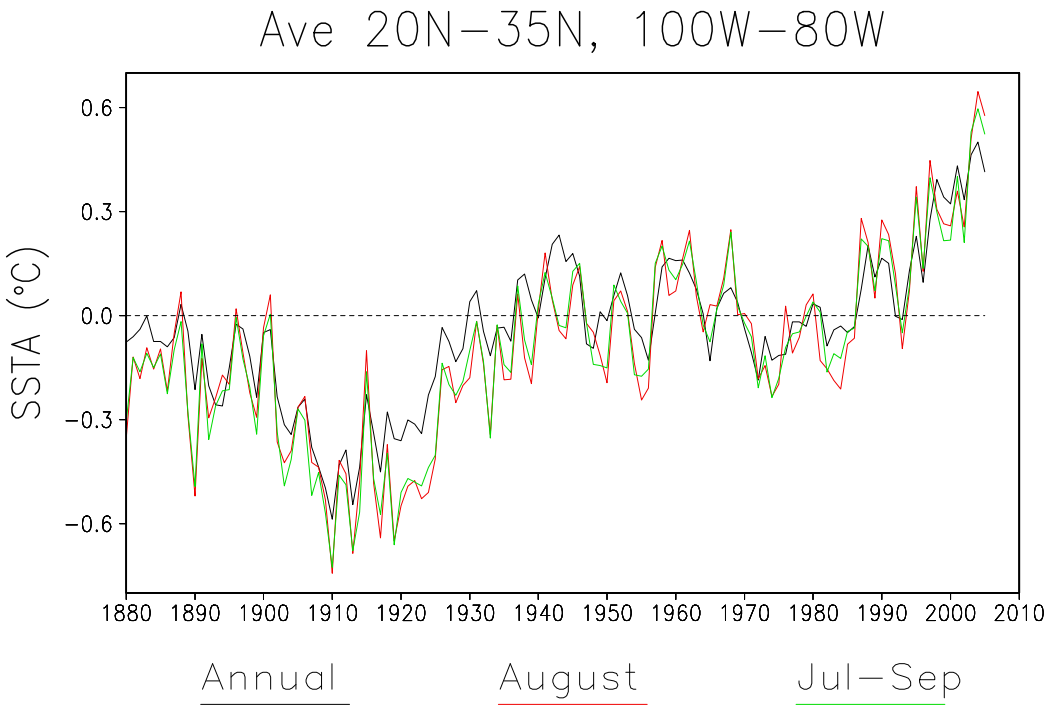

Figure 3.24 Satellite imagery of the Gulf of Mexico and warmer waters of the Loop Current that interacted with the track and storm strength of Hurricane Rita (2005). (Source: NASA/JPL/University of Colorado)

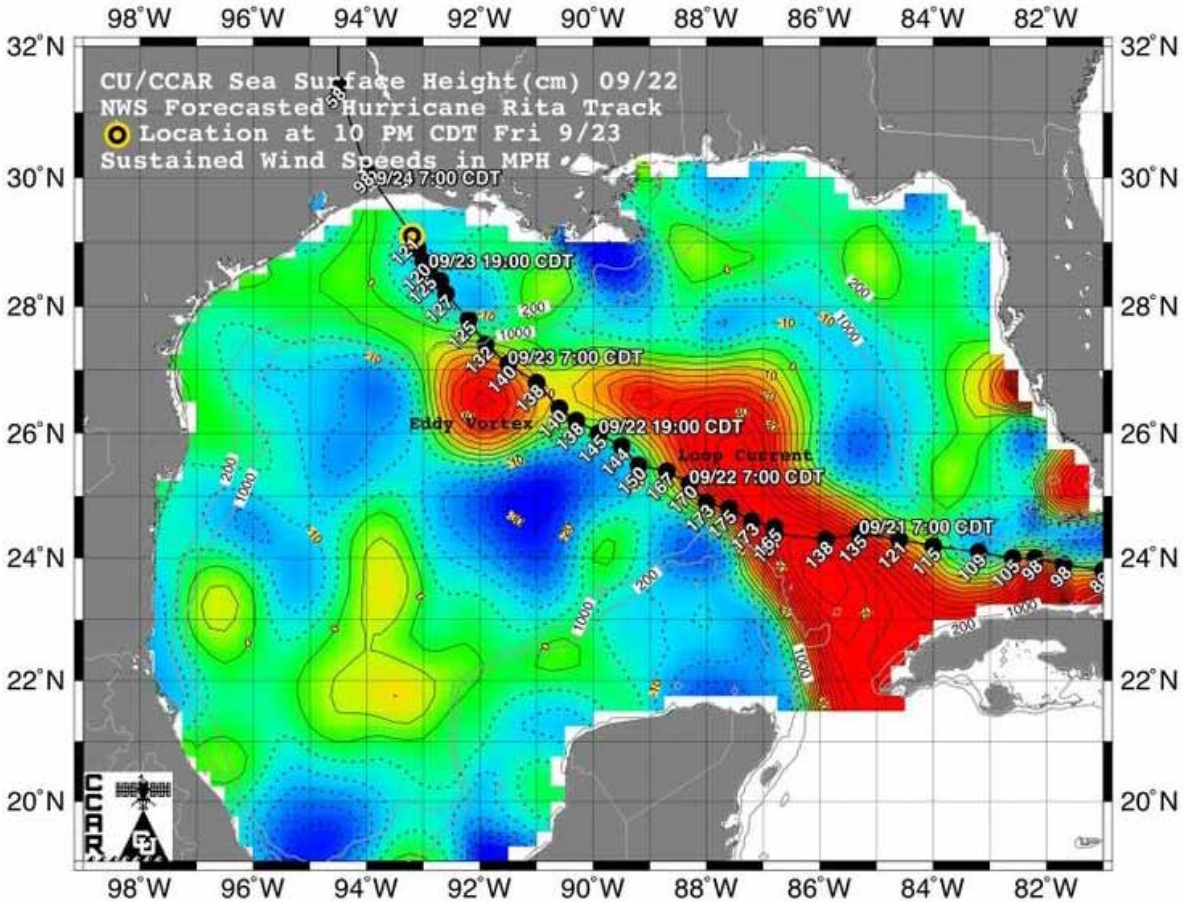

Figure 3.25 Frequency histogram of tropical storm events for coastal cities across the Gulf of Mexico region of the United States over the period of record from 1851 to 2006.

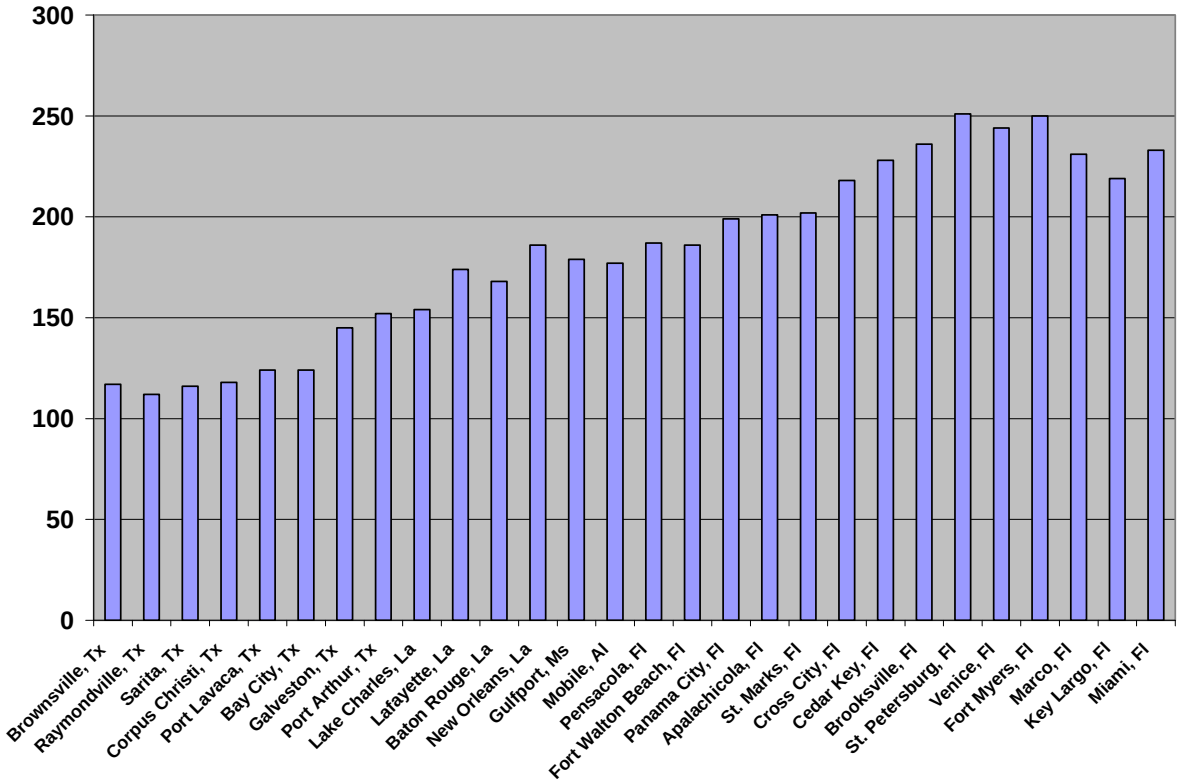

Figure 3.26 Frequency analysis of storm events exhibiting Category 1, 2, and 3 winds or higher across the Gulf Coast study area.

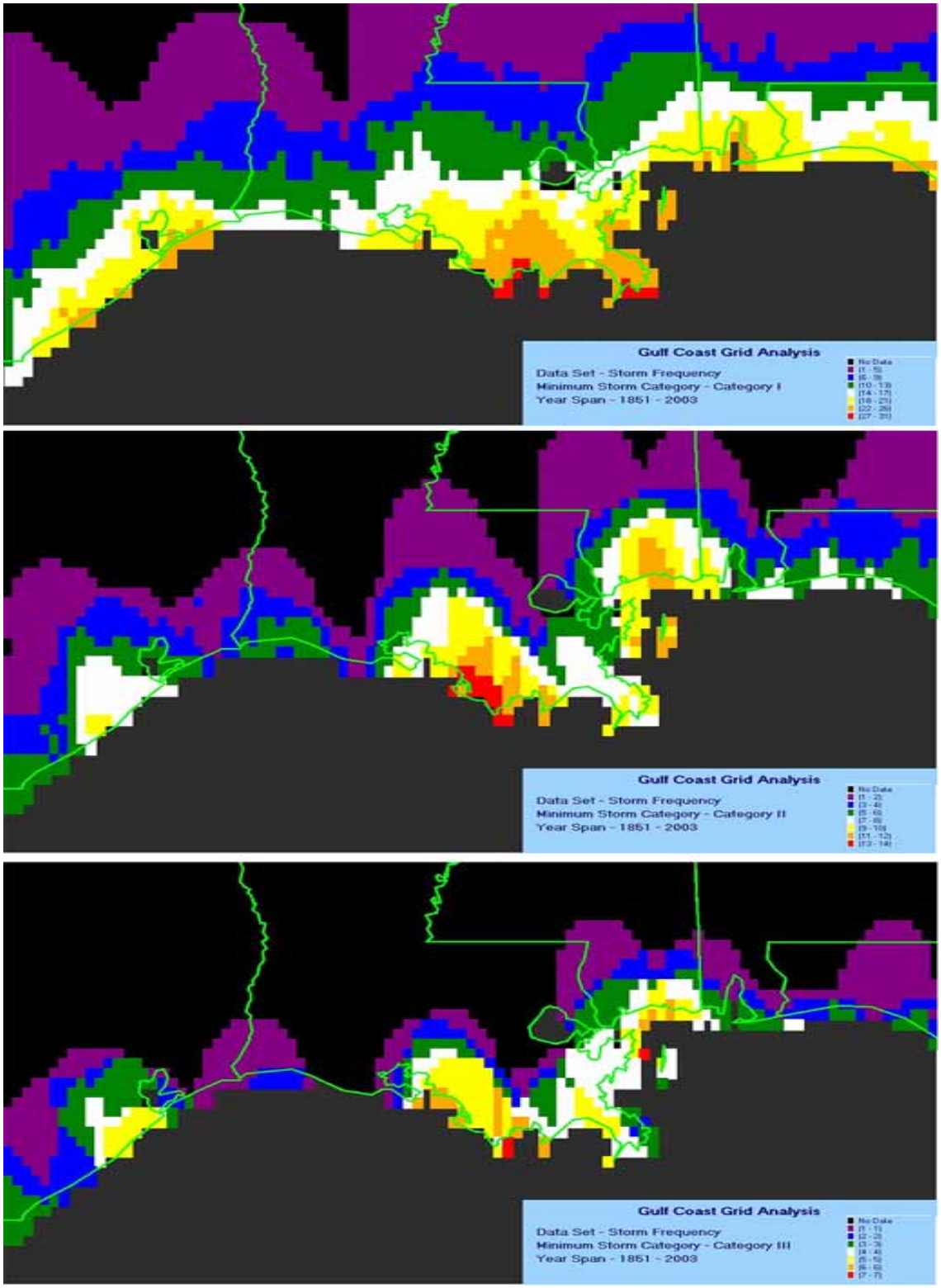

Figure 3.27 Latitudinal gradient of declining storm frequency of Category 1 hurricanes or greater from Grand Isle, LA inland illustrating the reduction of storm strength overland away from the coast, for the period 1951-2000.

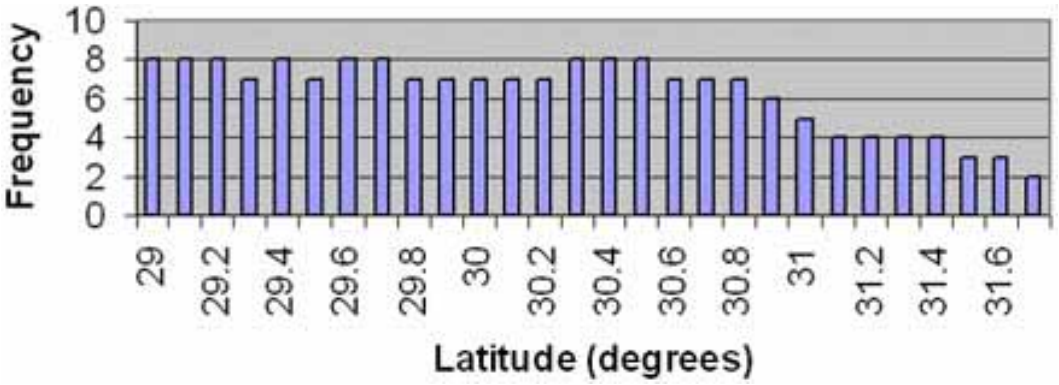

Figure 3.28 15-, 30-, and 50-year hurricane recurrence potential. Storm frequency variation for 15, 30, and 50 year intervals for Category 1 storms or greater for the most active grid location across the Gulf Coast study region.

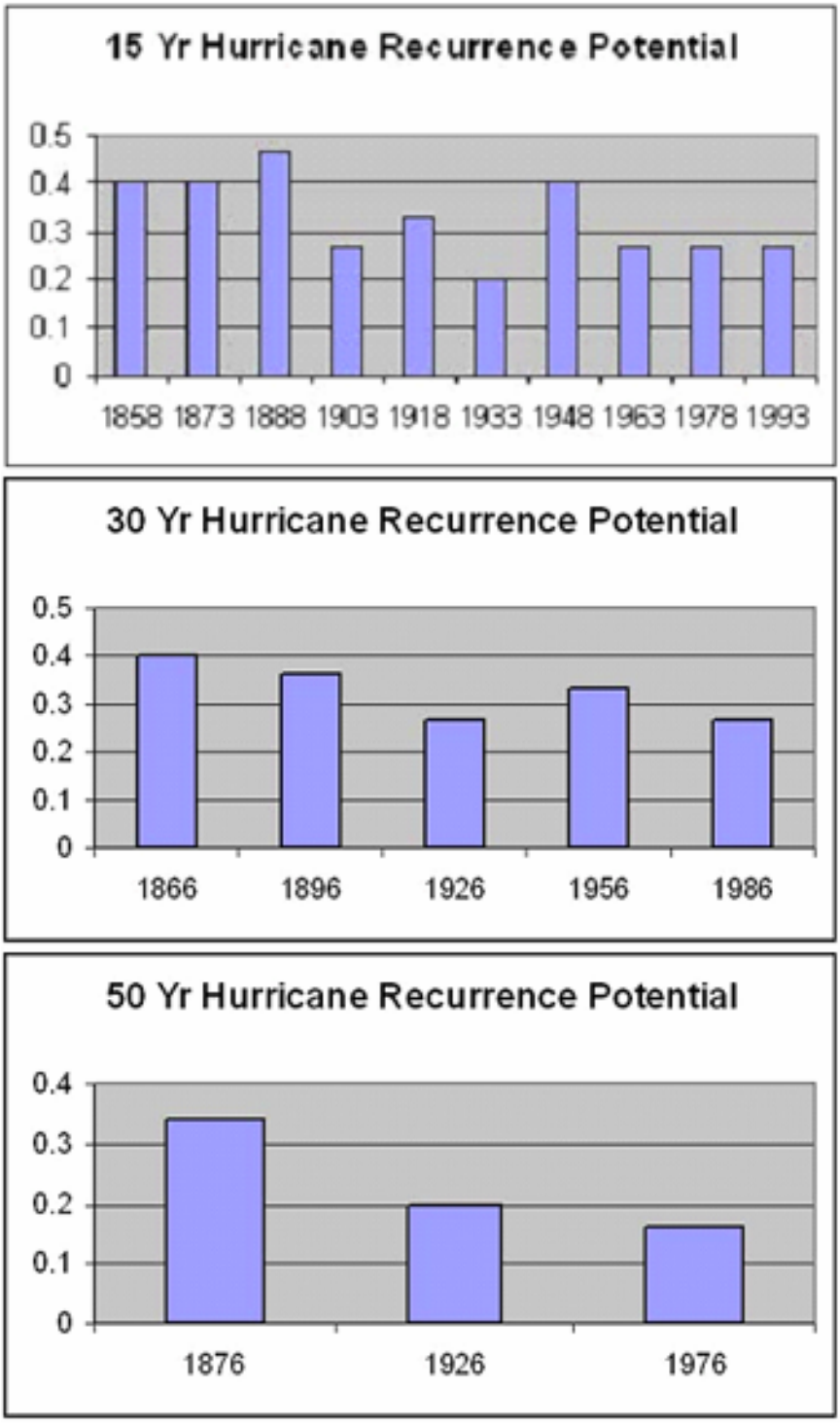

Figure 3.29 Simulated wind rows and direction of wind force derived from the HURASIM Model for one of the most active grid cell locations in the study area at Grand Isle, LA for tropical storm and hurricane conditions over the 153-year period of record.

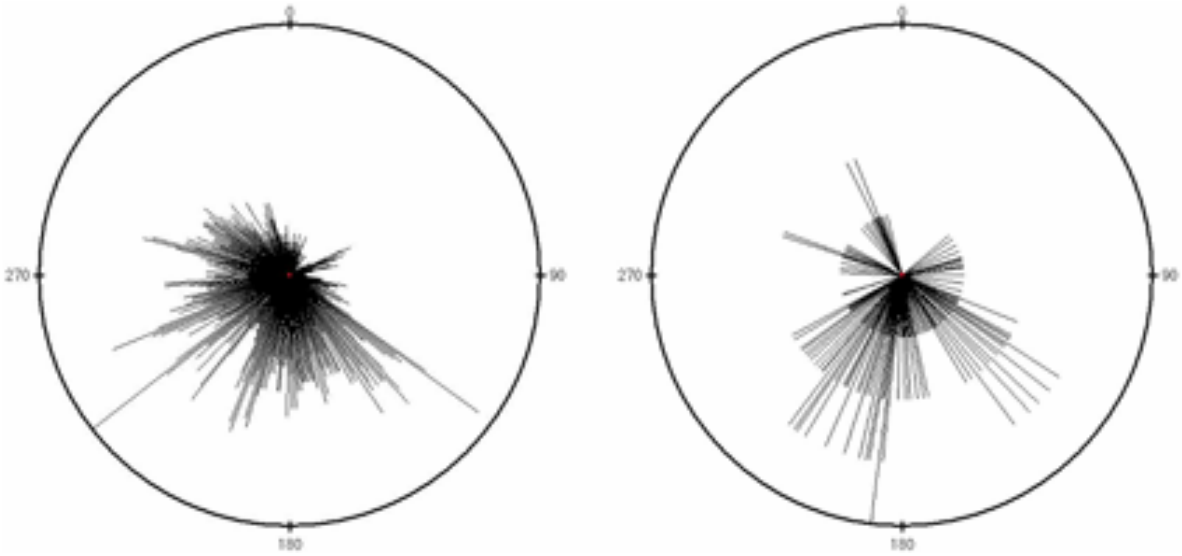

Figure 3.30 Potential increase in the number of hurricanes by the year 2050 and 2100 assuming an increase in hurricane intensity concomitant with warming sea surface temperatures projected at 5%, 10%, 15%, and 20%.

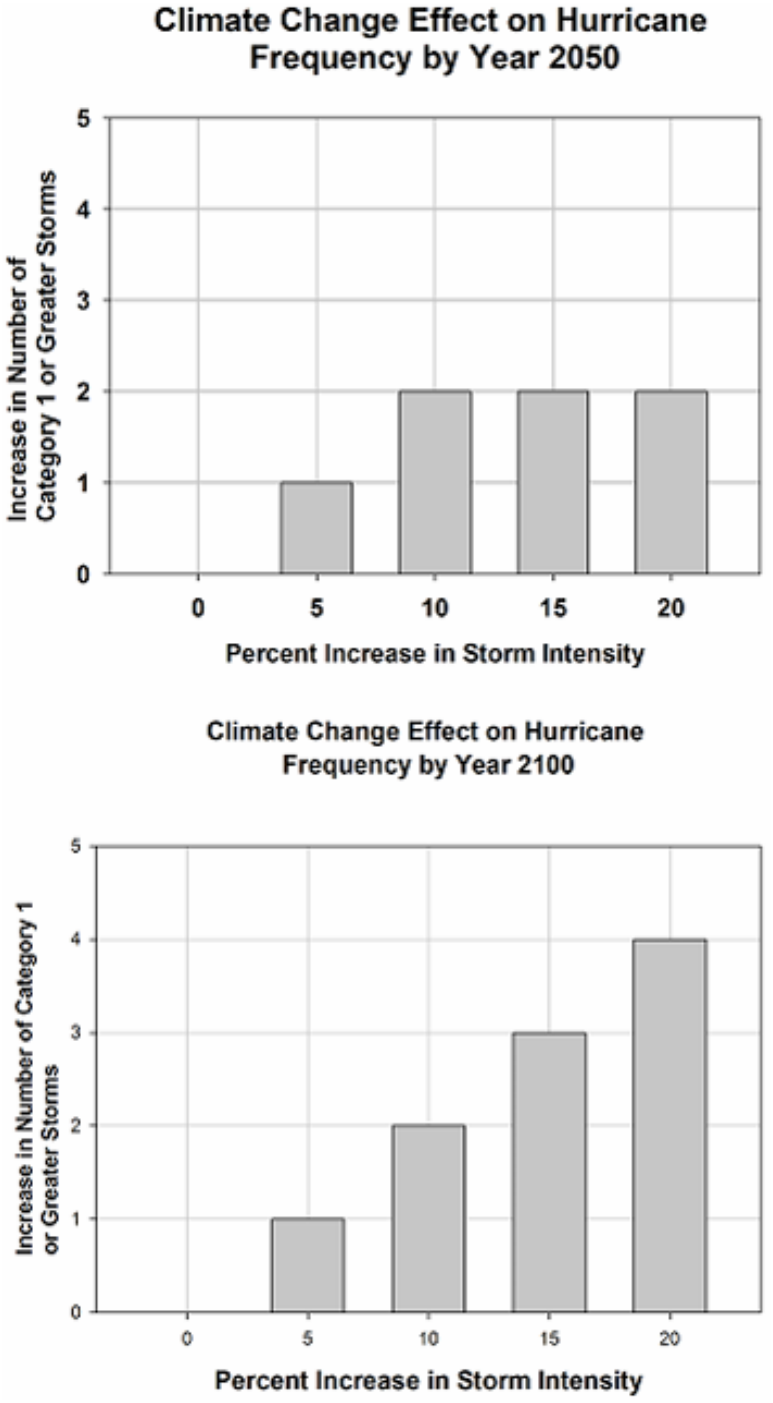

Figure 3.31 Tide gauge records and mean sea level trend line for three northern Gulf Coast tide stations at Pensacola, FL, Grand Isle, LA, and Galveston, TX corresponding with the eastern, central, and western coverage of the study area (1900-2000).

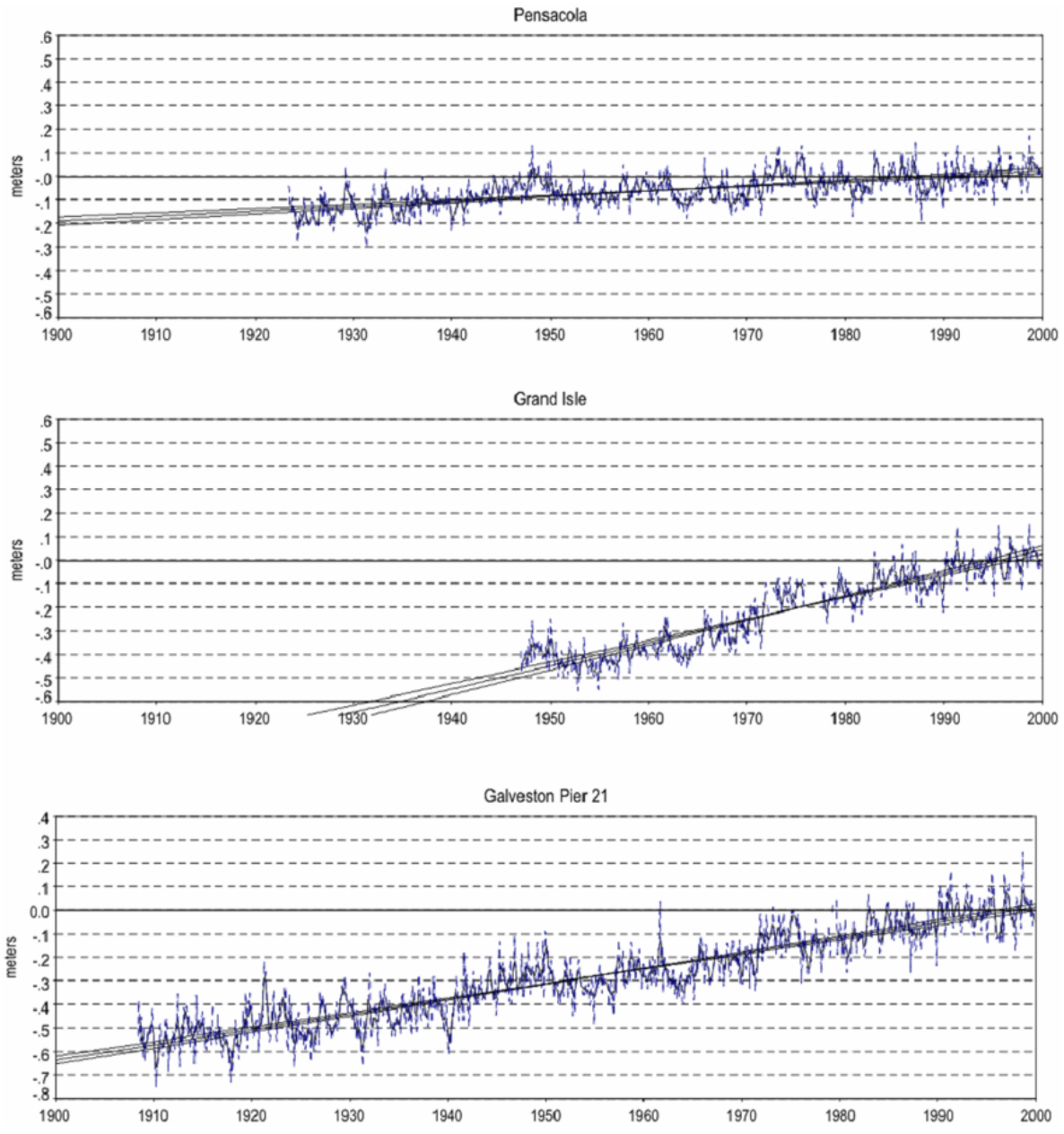

Figure 3.32 Sea level change curves from the CoastClim Model illustrating the projected sea-level rise including both land subsidence and future rates of eustatic rise for Low, Mid, and High Projections for all seven GCMs under the A1F1 scenario.

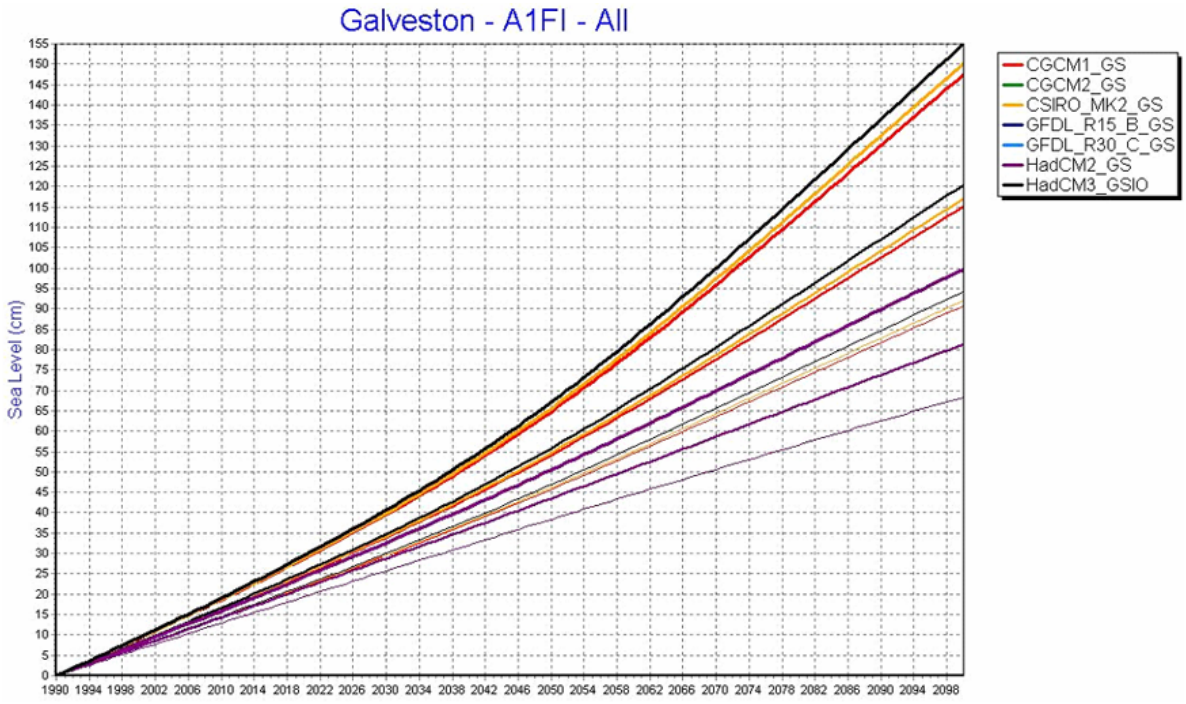

Figure 3.33 Merged results of Category 2 through 5 hurricane surge simulations of slow moving storm approaching from the southeast (toward northwest in database), using SLOSH model simulations.

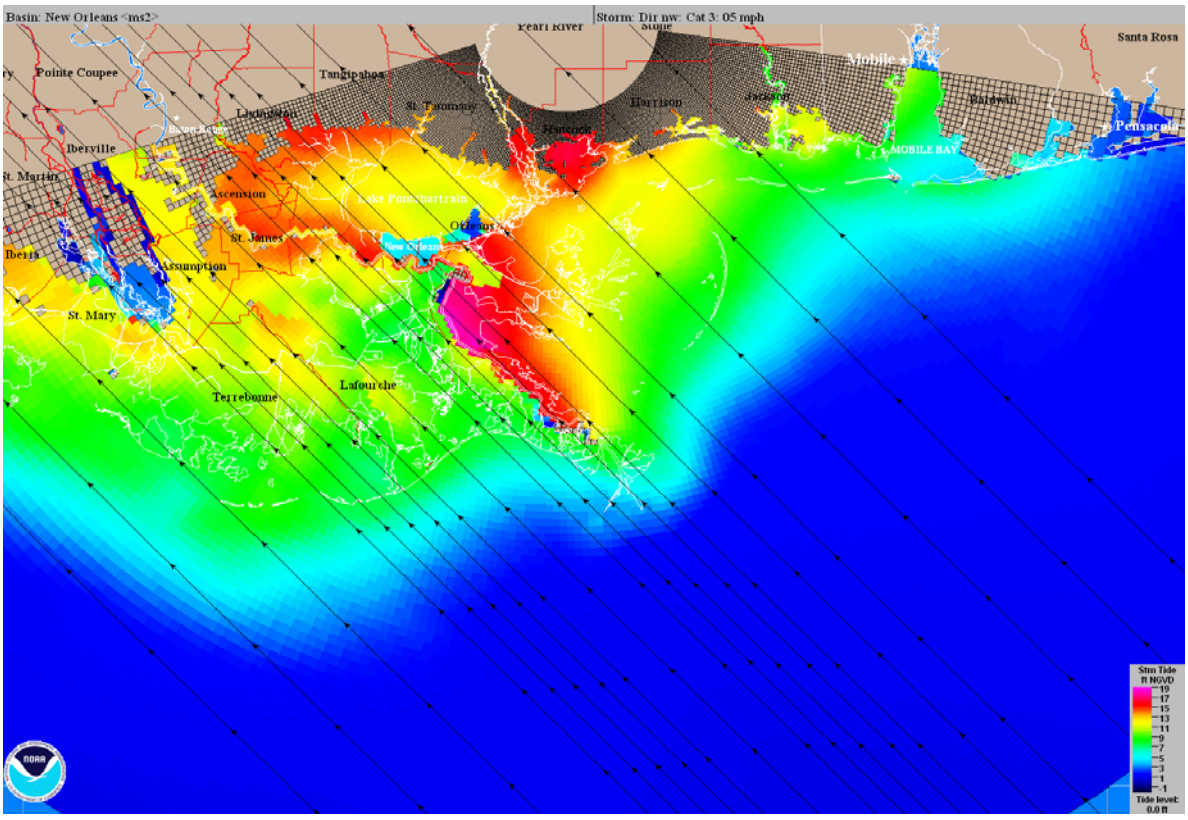

Figure 3.34 Color schemes illustrate the difference in surge inundation between a Category 3 and Category 5 storm approaching the southeastern Louisiana coast from the southeast.

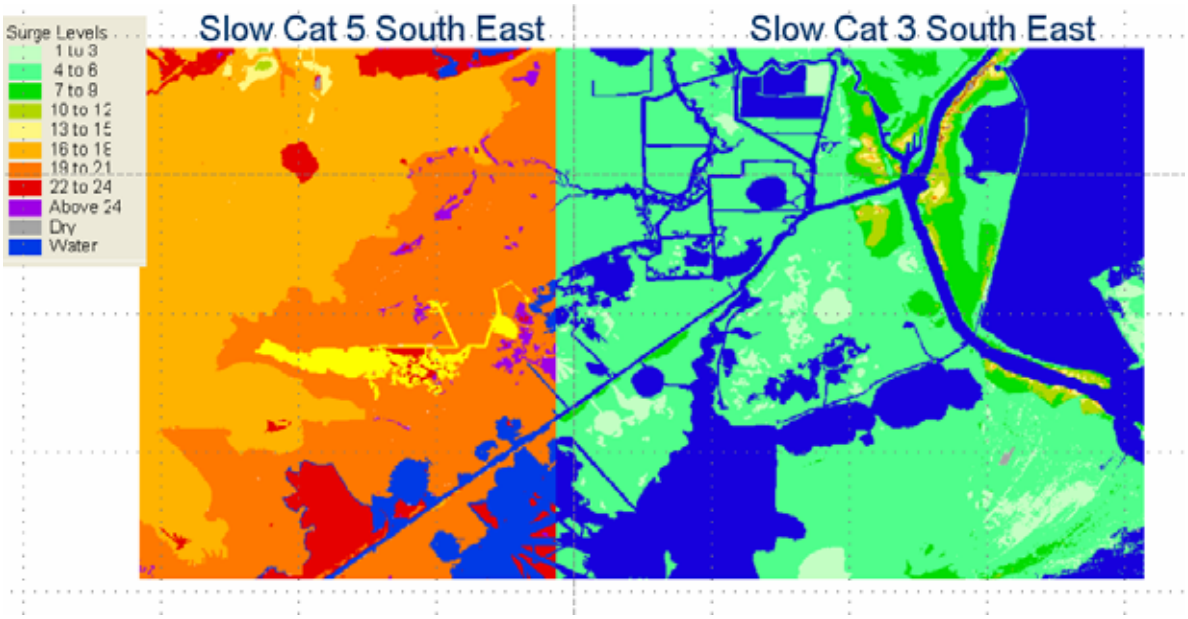

Figure 3.35 Comparison of Lidar and National Digital Elevation Data (DEM) for eastern Cameron Parish, Louisiana. The advantages of using a LiDAR-derived topography are many, particularly as the effects of climate change are likely to be subtle in the short-term but significant for this low-lying coast where 1 foot of added flooding will impact a large land area.

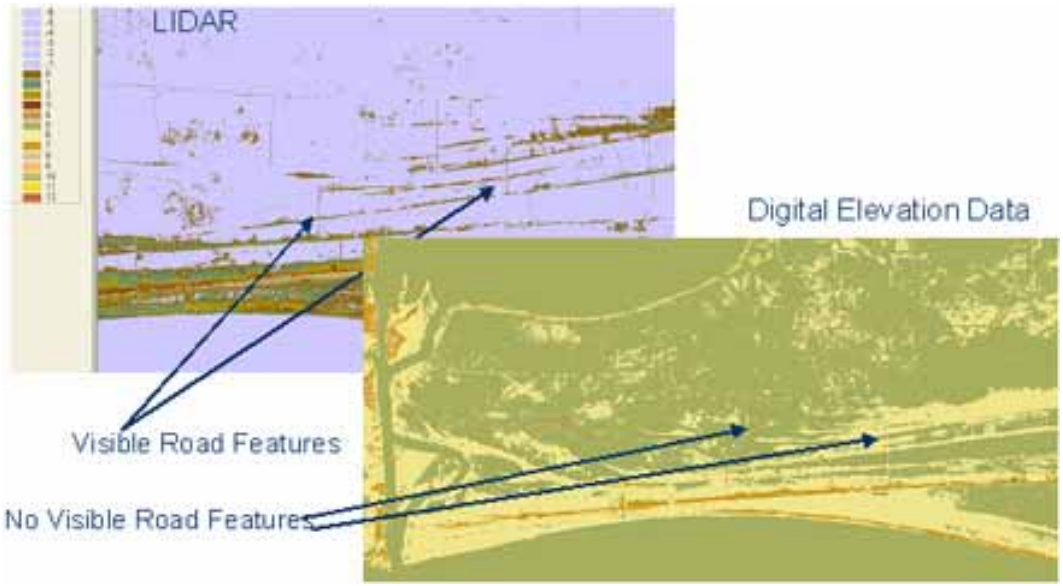

Figure 3.36 Trend in summer wave height (1978-2005) in the mid-Gulf of Mexico. (Figure source: Komar, in press; data source: National Buoy Data Center, NOAA, Stennis, Mississippi)